PNAS RESEARCH ARTICLE | APPLIED PHYSICAL SCIENCES

Spectroscopic evidence of spin-state excitation in d-electron correlated semiconductor $FeSb_2$

Huayao Li[a,1], Guohua Wang[b,1], Ning Ding[a,1], Quan Ren[a], Gan Zhao[a], Wenting Lin[a], Jinchuan Yang[b], Wensheng Yan[c], Qian Li[c], Run Yang[a], Shijun Yuan[a], Jonathan D. Denlinger[d], Zhenxing Wang[e], Xiaoqian Zhang[a], L. Andrew Wray[f], Shuai Dong[a,2], Dong Qian[b,g,h,2], and Lin Miao[a,2]

Affiliations are included on p. 5.

Edited by David Weitz, Harvard University, Cambridge, MA; received December 1, 2023; accepted May 28, 2024

Iron antimonide ($FeSb_2$) has been investigated for decades due to its puzzling electronic properties. It undergoes the temperature-controlled transition from an insulator to an ill-defined metal, with a cross-over from diamagnetism to paramagnetism. Extensive efforts have been made to uncover the underlying mechanism, but a consensus has yet to be reached. While macroscopic transport and magnetic measurements can be explained by different theoretical proposals, the essential spectroscopic evidence required to distinguish the physical origin is missing. In this paper, through the use of X-ray absorption spectroscopy and atomic multiplet simulations, we have observed the mixed spin states of $3d^6$ configuration in $FeSb_2$. Furthermore, we reveal that the enhancement of the conductivity, whether induced by temperature or doping, is characterized by populating the high-spin state from the low-spin state. Our work constitutes vital spectroscopic evidence that the electrical/magnetical transition in $FeSb_2$ is directly associated with the spin-state excitation.

X-ray spectroscopy | spin-state excitation | electronic correlation

Significance

Turning a metal into an insulator (and vice versa) by temperature is an important research field in physics and is essential for advancing information technology. Iron antimonide ($FeSb_2$) manifests mysterious MIT (metal-insulator transition)-like behaviors and record-breaking colossal thermoelectricity. This paper reports a comprehensive X-ray absorption spectroscopy study on $FeSb_2$, proving that Fe ions are in $3d^6$ configuration with mixed insulating low-spin (LS) state and metallic high-spin (HS) state. The profound enhancement of the conductivity, driven by either temperature or substitution, is consistently associated with populating in the HS state from the LS state. This work provides crucial evidence to support that electronic/magnetic transitions in $FeSb_2$ are directly associated with spin-state excitation.

Some compounds with partially filled *d*-orbitals, such as transition metal oxide or chalcogenide $LaCoO_3$, $NiS_{2-x}Se_x$, VO_2, and so on, are insulating at low temperatures, but with temperature-enhanced electrical conductivity driven by correlations arising from charge, orbital, spin, and even the intertwined degrees of freedom (1, 2). Among those insulators/semiconductors with partially filled *d*-shell, $FeSb_2$ has an insulating and diamagnetic ground state at low temperatures, manifesting the record-breaking colossal thermoelectric effect and puzzling resistance anomaly. When the temperature ramps up, the electrical resistivity of $FeSb_2$ is gradually diminished by more than five orders of magnitude, with the cross-over from diamagnetism to paramagnetism (3–6). Such exotic properties make people recall the metal-insulator transition (MIT-like), but lacking a clear transition point from the temperature-dependent resistivity (*R-T*) curve. Various theoretical approaches have been proposed to unveil the underlying mechanism of the transition from the insulating phase to the ill-defined "metallic phase" in $FeSb_2$. For instance, the insulating and diamagnetic nature of $FeSb_2$ (and correlated insulator FeSi) has been discussed as a consequence of the Kondo singlet ground state, and the closure of the gap is attributed to the melting of the Kondo singlet with increasing temperature (7–12). Some recent studies even claim that $FeSb_2$ and FeSi are probably topological Kondo insulators, resembling SmB_6 (13, 14). The spin-state excitation (SSE) mechanism has also been tentatively proposed to explain its MIT-like behaviors, in analogy to $LaCoO_3$, which is well known for its SSE-induced insulator-to-metal transition (4, 15–18). The temperature-controlled excitation from 3*d*-orbital low-spin (LS) state to the high-spin (HS) state would lead to the presence of delocalized electrons near the Fermi level, which is responsible for the itinerary and paramagnetism. For instance, High-field Mössbauer spectroscopy of hyperfine interaction within $FeSb_2$ also hinted at possibly two different spin components from a single valence condition (19). Unfortunately, theoretical models of totally different microscopic basis can not exclusively address the MIT-like phenomena of $FeSb_2$ just from the aspects of the macroscopic transport and magnetic measurements (3–9). Due to the lack of explicit and direct spectroscopic evidence, the physical origin of the MIT-like behaviors in $FeSb_2$ remains an open question.

In this work, we present a systematic X-ray absorption spectroscopy (XAS) study on $FeSb_2$ and slightly Ru-doped $FeSb_2$. With the help of atomic multiplet simulations (AMS), we revealed that Fe ions are in $3d^6$ configuration with mixed LS (S = 0) and HS (S = 2) states. The insulating LS state dominates the ground state at low temperatures. The enhancement of the conductivity, driven by either temperature or doping effect, is

Author contributions: S.D., D.Q., and L.M. designed research; H.L., G.W., N.D., Q.R., G.Z., W.L., J.Y., S.Y., J.D.D., Z.W., and L.M. performed research; W.Y., Q.L., and L.A.W. contributed new reagents/analytic tools; H.L., G.W., N.D., Q.R., R.Y., J.D.D., X.Z., S.D., D.Q., and L.M. analyzed data; and H.L., G.W., N.D., S.D., D.Q., and L.M. wrote the paper.

The authors declare no competing interest.

This article is a PNAS Direct Submission.

[1]H.L., G.W., and N.D. contributed equally to this work.

[2]To whom correspondence may be addressed. Email: sdong@seu.edu.cn, dqian@sjtu.edu.cn, or lmiao@seu.edu.cn.

This article contains supporting information online at https://www.pnas.org/lookup/suppl/doi:10.1073/pnas.2321193121/-/DCSupplemental.

Published July 2, 2024.

consistently associated with populating into the metallic HS state from the LS state. This direct observation provides compelling evidence that the MIT-like behaviors of $FeSb_2$ are closely correlated with the SSE within the framework of the HS/LS energy hierarchy.

Results

$FeSb_2$ crystalizes to a marcasite lattice (Fig. 1*A*) with the orthorhombic structure (space group *pnnm*). Under the CEF of distorted octahedral symmetry, Fe-3*d* orbitals form e_g and t_{2g} orbitals, and the energy degeneracy is further removed under the C_{2h} symmetry, as sketched in Fig. 1*B*. Early work claimed Fe is in a $3d^4$ configuration, occupying the lowest d_{xz}/d_{yz} orbitals (20, 21). Later, density-functional calculations and X-ray diffraction experiments suggested a divalent state of Fe ions due to the network of strong covalency (22–24). XAS is a powerful tool for studying the valence state of Fe ions. Fig. 2*A* presents the experimental (at 20 K) and simulated Fe *L*-edge XAS curves. Fig. 2*B* shows the second derivative curves of Fig. 2*A* to enhance the peak features for easy reading. The experimental data agree well with the simulated curves considering an LS $3d^6$ configuration but obviously deviate from the $3d^5$ or $3d^4$ outer shell configurations (*SI Appendix, Supplementary Note 1*). In the LS $3d^6$ configuration, the t_{2g} orbitals are fully occupied, as sketched in Fig. 2 *C*, *Left*, resulting in a zero spin moment (S = 0) and a multiplet energy gap. This coincides with the nonmagnetic insulating ground state of $FeSb_2$.

Although a fairly good agreement between the experimental and simulated results, the simulated XAS curve with 100% LS state does not fully reproduce the experimental XAS curve, as it fails to capture the prominent peaks at $h\nu$ = 705.7 eV ($h\nu$ = 718.7 eV) in the pre-edge region of the Fe-L_3 (Fe-L_2) main peak. Such pronounced pre-edge multiplet features are rarely seen in the XAS of $3d^6$ LS state with O_h CEF symmetry [e.g., iron-based superconductors (25, 26)] but were discovered in the previous XAS studies on $FeSb_2$ and other Fe-compounds with the HS state (e.g., FeO) (27–30). They were also tentatively claimed to result from a mixed-valence state without experimental confirmation (13). However, it is very unlikely since mixing with a $3d^5$ or $3d^4$ configuration would shift the XAS peaks to higher energy (*SI Appendix, Supplementary Note 1*) (28). Here, we found the $3d^6$ HS state is very crucial to reconciling the XAS results. The HS state (Fig. 2 *C*, *Right*) leaves vacancies in t_{2g} orbitals, so electrons are allowed to be excited from the core-level to t_{2g} orbitals, requiring less energy than the excitation to e_g orbitals in the LS state. Thus the $3d^6$ HS state gives rise to the XAS peaks shifting to lower energy (blue lines in Fig. 2 *A* and *B*). Considering a mixed spin state (~15% HS and ~85% LS) in simulations leads to pre-edge peaks in both L_3- and L_2-edges

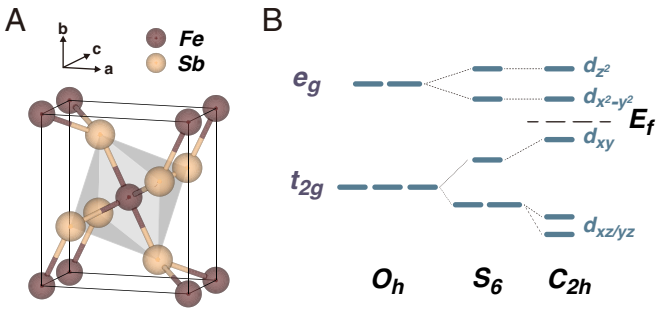

Fig. 1. $FeSb_2$ lattice structure and the energy levels of Fe-3*d* orbitals. (*A*) The unit cell of $FeSb_2$ lattice. (*B*) The energy levels of Fe-3*d* orbitals result from the CEF in a Marcasite lattice with C_{2h} symmetry (20). The Fermi level was noted as E_f.

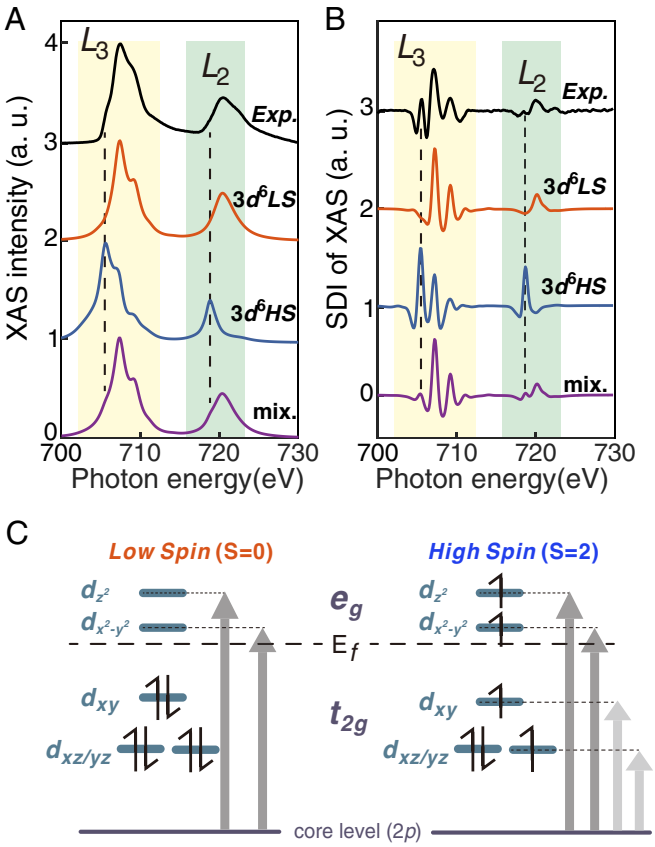

Fig. 2. The *L*-edge XAS and corresponding simulation of $FeSb_2$ and the spin excitation diagram. (*A*) The comparison of Fe *L*-edge XAS curves between experiments (black, T = 20 K) and the simulations of $3d^6$ LS state (red), HS state (blue), and the mixed spin state (purple, with 15% HS). (*B*) The second derivative images (SDI) of the experimental and simulated XAS curves. The vertical dashed lines mark the XAS peak ($h\nu$ = 705.7 eV and $h\nu$ = 718.7 eV) originating from the HS state. (*C*) The CEF split energy diagram of the Fe-3*d* orbitals in $FeSb_2$. All the t_{2g} orbitals are occupied for the LS state, forming an insulating state. For the HS state, t_{2g} and e_g orbitals are partially occupied, creating a metallic phase. The vertical arrows note the allowed possible transitions from the core levels to the vacant orbital. d_{xz}/d_{yz} orbitals are sketched here with degeneracy for simplicity. Please note that all the simulated and experimental XAS curves in this paper are normalized with the integrated XAS intensity from 700 eV to 730 eV. All XAS curves present in this figure is taken from (010) facet.

(solid purple curves in Fig. 2 *A* and *B*), significantly improving the agreement between the simulations and the experiments. Notably, a stable intermediate spin state (S = 1) would also partially occupy e_g orbitals and leave vacancies in t_{2g} orbitals. However, it requires a special CEF environment (such as Fe-molecular under square planar symmetry) (28), which is not the case in $FeSb_2$. Therefore, the presence of pre-edge peaks and the overall features of XAS support that $FeSb_2$ possesses a $3d^6$ configuration with a mixture of HS and LS states.

To investigate the correlation between the mixed spin state and the MIT-like transition, we performed temperature-dependent XAS measurements from T = 20 K to T = 300 K. The XAS curves of different temperatures appear quite similar (Fig. 3*A*), but the temperature-dependent contrast becomes apparent (Fig. 3*B*) after subtracting the XAS curve of 20 K from other XAS curves. Within the L_3-edge region, a prominent feature with positive intensity is observed at around $h\nu$ = 705.7 eV, corresponding to the energy position of the HS state in Fig. 2*A*. This positive feature is incremental with the temperature. Meanwhile, two dips with negative intensities were observed at about $h\nu$ = 707.5 eV and $h\nu$ = 709.4 eV at high temperatures, matching the energy positions of two prominent peaks of the LS state in Fig. 2*A*. The appearance of dips means the decrease

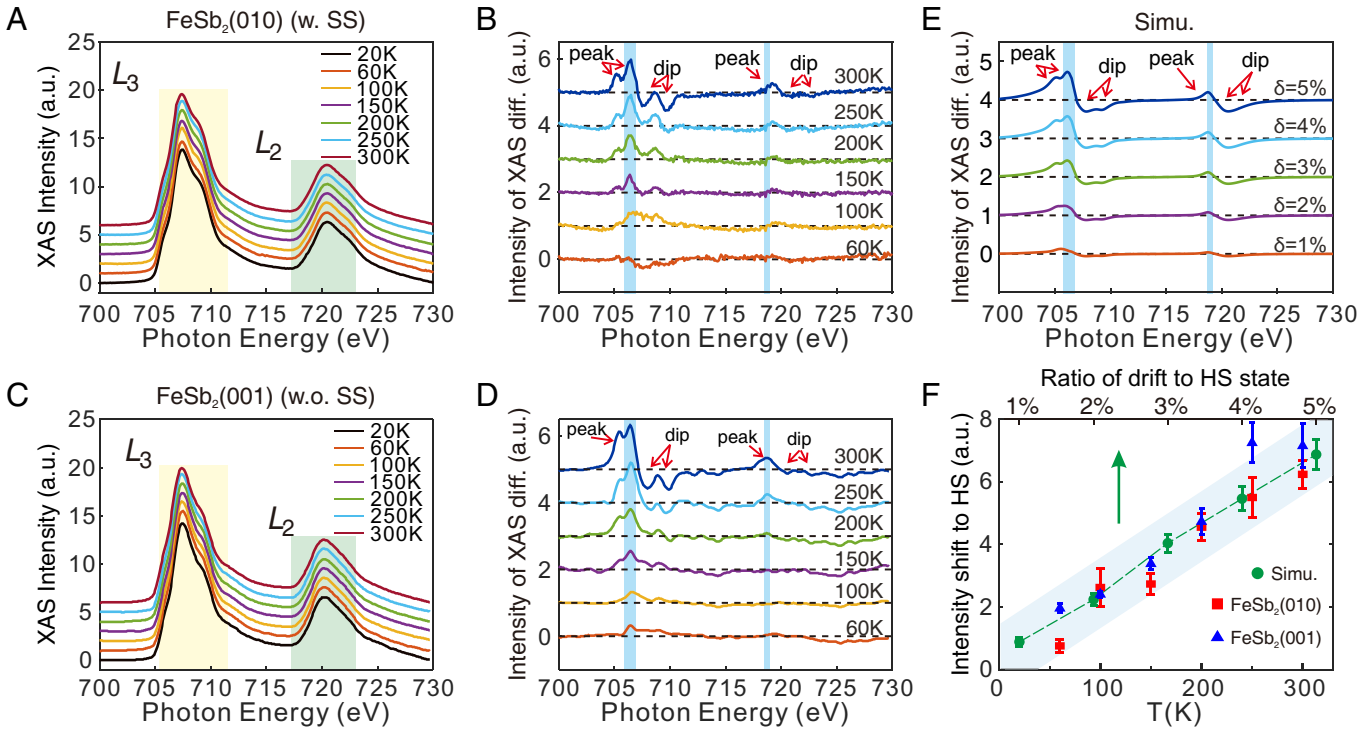

Fig. 3. Temperature-dependent XAS measurements and simulations. (*A*) The XAS curves of $FeSb_2$ (010) at different temperatures (from 20 K to 300 K). The XAS was measured during the warming-up process to eliminate the errors in reading the temperature. (*B*) The temperature-dependent differentiated $FeSb_2$ (010) XAS curves after subtracting the XAS curve of T = 20 K ($I_{(T)}$-$I_{(20K)}$). (*C*) Separated T-dependent XAS was measured on $FeSb_2$ (001), which is without electronic SS. (*D*) The T-dependent differentiated $FeSb_2$ (001) XAS after subtracting the XAS curve of T = 20 K ($I_{(T)}$-$I_{(20K)}$). (*E*) The simulated differentiated XAS curves after subtracting the XAS curve with 15% HS state. Red arrows note the peaks and dips. More simulation details can be found in *SI Appendix, Supplementary Note V*. (*F*) The XAS intensities shifted from the LS state to the HS state extracted from experiments (red/blue) and simulations (green) (*Left* axis), and the corresponding ratio of HS state populated from low temperature to 300 K (*Top* axis). The shifted intensities are sampled by integrating the intensity of blue-shaded ranges in L_3-edge (705.8 eV to 706.8 eV) and L_2-edges (718.5 eV to 719 eV) of the differentiated XAS from (*B*), (*D*) and (*E*).

in the LS state. The gain of the HS state's intensity is simultaneously along with the loss of intensity in the energy regime of two dips, indicating the drift from the LS state to the HS state. A similar behavior exists in the L_2-edge, although the signals of peaks and dips are weaker. We notice that magnetic circular dichroic (XMCD) measurements on an unspecified sample's surface in ref. 27 are incompatible with the magnetic susceptibility, indicating possibly a bulk-surface separation. If so, these XAS peaks might come from the electronic surface states (SS), which are identified at the surface of $FeSb_2$(010) and (110) facets (13, 24, 31). To rule out the possibility that what we observed is an effect resulting from the electronic SS resident on $FeSb_2$ (010) facet (13, 24), we repeated the same measurements on the cleaved surface of (001) facet (Fig. 3 *C* and *D*), which is identified to be free from any SS by high-resolution angle-resolved photoemission spectroscopy (ARPES, see *SI Appendix, Supplementary Note II*). The highly identical results from the (001) and (010) facets suggest that the drift of spin states is not induced by SS. The seeming mismatch between the magnetic susceptibility and the XMCD in ref. 27 is interesting, but would possibly be addressed if more experimental information and analysis were provided in that work. Furthermore, temperature-cycled XAS measurements confirm the changes of XAS as temperature dependence is reversible (*SI Appendix, Supplementary Note III*). The T-dependent XAS measurements were performed on a separate crystal (namely, sample #2) to show the same behaviors, indicating it is an intrinsic property of $FeSb_2$ (*SI Appendix, Supplementary Note IV*).

Moreover, we simulated the XAS curves by increasing the ratio of the HS state to catch the fine distinctions of T-dependent XAS (see more details in *SI Appendix, Supplementary Note V*). Fig. 3*E* presents the simulated results, which were differentiated between the XAS of increasing HS state ratio (from 16 to 20%) and the base XAS with an HS state of 15%. Consistent with experiments, the simulated differentiated XAS curves also show peak-dip features at the characteristic energies in both L_3 and L_2-edges (Fig. 3*E*). A quantitative assessment of how much the ratio of LS state drifted to the HS state from 20 K to 300 K is then evaluated. By integrating the intensity of the peaks of experimental data (blue-shaded ranges, Fig. 3 *B* and *D*), we can trace the change of HS state's intensity as a function of temperature (red squares and blue triangles in Fig. 3*F*). In the meantime, using the simulated data in Fig. 3*E*, one can also extract the corresponding intensity of the HS state (blue-shaded ranges) as a function of the HS state ratio change, and compare it directly with the experimental results (Fig. 3*F*). The increase of the spectral weight of the HS state from 20 K to 300 K can be fitted well by raising the ratio of the HS state approximately from 15 to 20%. Yet, one needs to be very cautious when interpreting the quantitative assessment (5% increment of HS) due to the limitation of the AMS. Nevertheless, the coordinative results from both experiment and simulation successfully depict the picture of SSE from LS to HS during the transition from insulating to conducting state.

Despite the temperature, the substitution of Fe-ions could also tune the $3d^6$ spin state and the corresponding electrical properties of $FeSb_2$. Slightly substituting Fe with ruthenium (Ru) would not alter the crystal structure since $RuSb_2$ is isostructural to $FeSb_2$. As shown in Fig. 4*A*, the 5% Ru-doped sample retains the MIT-like behavior (see magnetic susceptibilities shown in *SI Appendix, Supplementary Note VI*). The absolute resistivity becomes larger (*Inset* of Fig. 4*A*) in doped samples, which is possibly due to doping-induced disorders. In contrast, the resistance ratio value ($R_{(2K)}/R_{(300K)}$) was reduced by about ~4 times after Ru doping (Fig. 4*A*). The resistance anomaly at T < 5 K was found in both

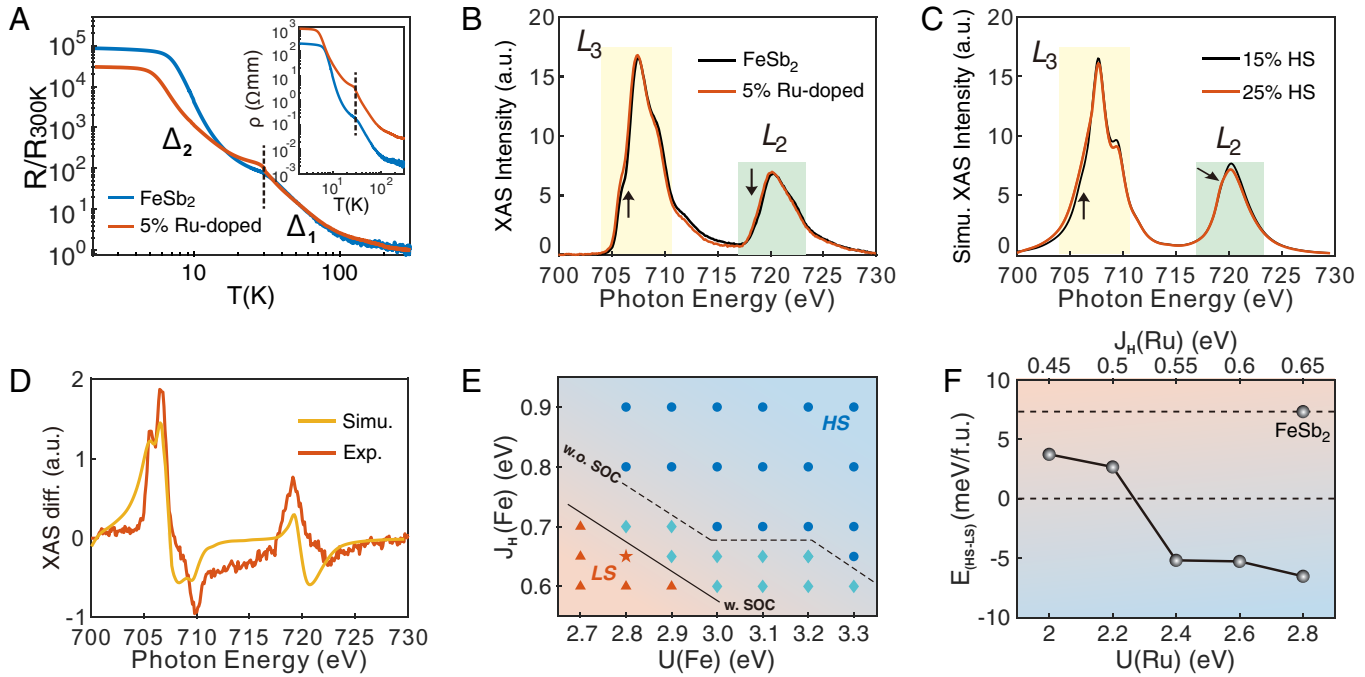

Fig. 4. Electrical transport, XAS measurements, and first-principles calculations on the Ru-doped $FeSb_2$. (*A*) The normalized resistance (R/R_{300K}) of $FeSb_2$ (blue) and $Fe_{0.95}Ru_{0.05}Sb_2$ (red) as a function of temperature. The vertical dashed line at T = ~30 K marks the temperature value where the system transits from a larger energy gap (Δ_1) to a smaller energy gap (Δ_2). The *Inset* shows the resistivity. (*B*) The XAS curves of $FeSb_2$ (black) and Ru-doped $FeSb_2$ (red) at T = 20 K. (*C*) The comparison of simulated XAS curves of different HS state ratios [15% (black), 25% (red)]. Black arrows in (*B* and *C*) indicate the photon energy where the XAS intensity changes. (*D*) The comparison of differentiated XAS ($XAS_{(Ru\text{-}doped)}$-$XAS_{(pristine)}$, red) with simulated differentiated XAS. The simulated differentiated XAS was generated by subtracting the XAS curve of 25% HS state from the XAS curve of 15% HS state. (*E*) The spin-state phase diagram of $FeSb_2$ in the parameter space of Fe's U and J_H. The blue dots (red triangles) indicate that the ground state is the HS (LS) state regardless of whether the SOC effect is taken into account. The cyan diamonds indicate a transition region where the ground state is the LS state without SOC but the HS state with SOC. The red star indicates the selected U and J_H when calculating Ru-doping. (*F*) The energy difference between the HS and LS states ($E_{(HS\text{-}LS)}$) changes with the Ru-dopants' U/J_H values. The J_H/U strength is roughly fixed as ~0.23.

samples, which is possibly a result of the in-gap SS identified in $FeSb_2$, resembling the similar feature in SmB_6 (13, 24, 31, 32). Meanwhile, the *R-T* curves of both samples share the same kink feature at T ~ 30 K to separate two regimes, dominated by different energy gaps (Δ_1 and Δ_2) (3–7, 13, 32, 33). The larger gap Δ_1 (above 30 K) is widely accepted as the intrinsic multiplet gap of Fe 3*d*-orbital, while the physical origin of the smaller one Δ_2 (below 30 K) is still controversial. It was claimed that Δ_2 might present the excitation of impurity states within the CEF gap (34, 35). However, the indirect excitation nature supports it could be an intrinsically correlated gap (33, 36). In our experiments, both gaps of each sample were extracted by fitting the *R-T* curves by using the Arrhenius equation $R \sim Ae^{\frac{\Delta}{2k_BT}}$, and both gaps are shrunken after the Ru-doping (*SI Appendix, Supplementary Note VI*). The multiplet gap Δ_1 is about 33.4 meV for $FeSb_2$ but 30.6 meV after doping with Ru. The gap Δ_2 is about 10.4 meV for $FeSb_2$ and 6.3 meV for Ru-doped $FeSb_2$. The reduction of Δ_1 after 5% Ru-doping indicates a smaller $3d^6$ multiplet gap between the t_{2g} and e_g states. Since the CEF splitting is a key factor in tuning the competition between the LS and HS states, the reduced CEF gap would favor the HS state. Therefore, one would anticipate a gain in the HS state in the XAS measurement on Ru-doped samples. The XAS of Ru-doped $FeSb_2$ shows an apparent increase in intensity at the characteristic energy position of the HS state (Fig. 4*B*), which can be reproduced by simulation with a larger portion (25%) of HS state (Fig. 4*C*). Meanwhile, increment of 10% HS (from 15 to 25%) also very well fits the differentiated XAS curve in Fig. 4*D*. Although the increased HS state ratio with the shrunken multiplet gap in Ru-doped samples is in line with the SSE narrative, the exact reason why the HS ground state is substantially enhanced by Ru-dopants needs to be well understood quantitively.

Therefore, to explore the associated energy scales and the underlying mechanism of how 5% Ru-dopants greatly boost HS state occupations, we performed first-principles calculations. A phase diagram (Fig. 4*E*) is obtained in the parameter space of the Hubbard U and Hund's coupling J_H. It is expected that the LS state (red-shaded) is preferred in the low U-J_H region, while the HS (blue-shaded) occupies the high U-J_H region. An important message is that the spin–orbit coupling (SOC) promotes the HS state, by pushing the LS-HS phase boundary to the low U-J_H direction. According to this phase diagram and experimental results, we adopted U = 2.8 eV/J_H = 0.65 eV as a proper set of parameters to describe $FeSb_2$, which leads to the LS state near the phase boundary and a semiconductor gap (Δ_1) of ~50 meV. The energy difference between the HS and LS states is rather tiny as $E_{(HS\text{-}LS)}$ ~ 7.5 meV/f.u. Then, the spin ground state of Ru-doped $FeSb_2$ is also surveyed as the function of Ru-dopants' U-J_H. Since the SOC can promote the HS state (Fig. 4*E*) and Ru's SOC is larger than Fe's, it is reasonable to expect the SOC-driven HS tendency. As shown in Fig. 4*F*, the $E_{(HS\text{-}LS)}$ value gradually shrinks with low U-values and the ground state can even flip to HS with higher U-values. By considering the larger extension of the Ru 4d-orbitals, it is well accepted that the U-J_H of 4d orbitals should be notably smaller than the 3d ones. Consequently, the smaller U/J_H, e.g., U = 2.2 eV/J_H = 0.5 eV, should reasonably fit the LS ground state. Furthermore, the significantly dampened $E_{(HS\text{-}LS)}$ ~ 2.5 meV/f.u. is comparable to the small thermal activation energy of T ~ 20 K, which explains why Ru-dopants greatly enhance the HS state occupation.

Although the SSE narrative is based on a framework nearly degenerate HS-LS state, Our experiments and calculations suggest that CEF energy and Hund's rule repulsion are not the sole factors in determining which spin state (LS or HS) dominates the ground state (24, 37). The SOC effect which favors the HS state, must also be considered. For a given SOC strength, a dedicated balance would be reached when the CEF splitting competes with a strong Hund's correlation. It is known that Hund's coupling is weakly dependent on temperature (38). CEF energy is inversely related to the lattice volume and usually slightly weakens under the lattice thermally expansion. When the energy difference between the LS and HS ground states is rather small (or nearly degenerate, namely), thermally activation energy could stand out to tune the occupation of HS/LS states and the metallic/insulating state.

Meanwhile, the physical origin of the mixed LS-HS ground state in $FeSb_2$ is an interesting question. The spin-state transition identified in the other compounds like $LaCoO_3$ is inevitably derived from the change of local chemical environment like the bond-state and lattice structure (39). The lattice distortion of $FeSb_2$ has been reported (7, 40), but with a clear difference when compared to $LaCoO_3$. The change of bond length within $LaCoO_3$ is continuous to even T ~ 1,000 K (39). However, the detected lattice distortion in $FeSb_2$ is more complicated. Despite thermally induced lattice expansion, an abrupt lattice distortion happened at T ~ 100 K in $FeSb_2$ by Raman spectroscopy, which is likely related to the lattice symmetry along the a-axis (40). It was argued that the symmetry changes at T ~ 100 K would trigger the spin state excitation (7). However, the photoemission results suggest a continuous change of electronic band structure from ~20 K to ~200 K (13, 24), which is in line with our XAS result. Previous XAS/RIXS work of $LaCoO_3$ shows that the HS state is populated to more than 50% at T ~ 300 K, which is profoundly larger than the ratio of 5% extracted by AMS in $FeSb_2$. Here, we'd like to reiterate the limits of AMS in quantitatively accessing the spin-state ratio in $FeSb_2$. Furthermore, the excitation of spin-unpaired electrons has been detected by high-field electron paramagnetic resonance spectroscopy in $LaCoO_3$ (41), but was absent in $FeSb_2$ (*SI Appendix*, *Supplementary Note VII*). Therefore, $FeSb_2$ should not be viewed as a straightforward analog of $LaCoO_3$, and more research is needed to determine whether the observed LS-HS excitation is the only mechanism involved in modulating the electric/magnetic properties.

Conclusion

To conclude, our comprehensive study on $FeSb_2$ and the analysis of its spin state reveal that $FeSb_2$ has a $3d^6$ mixed spin state with equilibrium between S = 0 and S = 2. The enhanced conductivity either tuned by temperature or doping is strongly associated with the drift from the insulating LS state to the metallic HS state. Our work supports the SSE mechanism, instead of the Kondo correlation, which plays an important role in tuning the electrical properties in $FeSb_2$. Finally, it is noteworthy that figuring out the orbital occupancy/spin state is the first step to fully understanding the mysterious properties of $FeSb_2$. For instance, the record-breaking colossal thermopower is deeply rooted in the electronic structure near the Fermi level (40, 42). The determined low-energy electronic structure could also help realize the altermagnetism in Co-doped $FeSb_2$ (43). Meanwhile, The SSE mechanism of MIT-like behaviors in $FeSb_2$ will have substantial implications for other mysterious iron-based correlated materials like FeSi or $FeGa_3$ (12, 44) that exhibit similar macroscopic properties as $FeSb_2$.

Materials and Methods

The single crystals of $FeSb_2$ and Ru-doped $FeSb_2$ were grown by a self-flux method, the same as ref. 5. They are cleaved in the ultrahigh vacuum with a base pressure better than 2×10^{-9} torr to obtain clean (010) and (001) surface for spectroscopic study. The soft X-ray absorption (Fe *L*-edge) spectroscopy measurements were performed in the Beamlines MCD-A and MCD-B (Soochow Beamline for Energy Materials) at National Radiation Source Lab (Hefei). The X-ray was with π polarization, and the data were collected with the total electron yield mode. AMS of XAS were performed as in refs. 25, 45, and 46, describing $2p^6\,3d^n \rightarrow 2p^5\,3d^{n+1}$ (Fe *L*-edge) X-ray absorption in the dipole approximation. Hartree–Fock parameters were obtained from the Cowan code (47), and full diagonalization of the multiplet Hamiltonian was performed using LAPACK drivers (48). The *d*-shell interaction (F_{dd}) was renormalized as 80% and the crystal field splitting energy (CEF, 10Dq value) was set to 2.0 eV to generate a $3d^6$ LS ground state. Meanwhile, the 10Dq was lowered to 1.8 eV to gain pure $3d^6$ HS ground states. All the other parameters remain intact and identical between the HS and LS state simulations to exclude the uncertainties induced by tuning other parameters. However, we notice that HS/LS states would generate different core-hole energies. Thus, the simulations of divalent Fe HS state and LS state are toy models based on the large CEF and relatively smaller CEF scenarios (with the cross-over 10Dq = 1.87 eV) to illustrate only the framework of SSE.

The first-principles calculations based on density functional theory (DFT) were performed with the projector augmented wave pseudopotentials as implemented in the Vienna ab initio Simulation Package (49, 50). The plane-wave cutoff energy was 500 eV, and the Fe's $4s3d3p$ electrons were treated as valence states. The *k*-point grid of 6 × 5 × 10 was adopted for the smallest primitive cell. A criterion of 0.01 eV/Å was used for the Hellman–Feynman forces during the structural relaxation and the energy convergency criterion is 10^{-6} eV. The Perdew–Burke–Ernzerhof parametrization of generalized gradient approximation was used for the exchange-correlation function (51). In order to describe the strongly correlated *d*-electrons from the iron element, the rotationally invariant DFT+*U* without exchange splitting introduced by Liechtenstein (LDAUTYPE=4) was taken into consideration (52), where the effective on-site Coulomb parameter (U) and exchange parameter (J_H) can be adjusted. The Ru doping was done in a 2 × 2 × 2 supercell with a concentration of 6.25%, close to the 5% doping ratio in the experiment.

The ARPES measurements in *SI Appendix, Supplementary Note II* note were performed at the MERLIN ARPES endstation beamline 4.0.3 at the Advanced Light Source and BL03U of Shanghai Synchrotron Radiation Facility. The temperature was maintained at T = 20 K, and the overall energy and resolution were 15 ~ 20 meV. The base pressure is better than 1×10^{-10} Torr. All ARPES data were taken within 10 h after cleavage, and band structure was stable on this timescale.

Data, Materials, and Software Availability. All study data are included in the article and/or *SI Appendix*.

ACKNOWLEDGMENTS. This work was supported by the National Key R&D Program of China (No. 2021YFA1400100, No. 2022YFA1405700, and No. 2022YFA1402400), National Natural Science Foundation of China (No. 12374058, No. 12074248, No. 12325401, No. 12004071, and No. U2032156), the program of Jiangsu specially appointed professor and Jiangsu Funding Program for Excellent Postdoctoral Talent. This research used resources of the Advanced Light Source, which is a Department of Energy Office of Science User Facility under contract no. DE-AC02-05CH11231. This work also used the resources of the Shanghai Synchrotron Radiation Facility, which is supported by SiP.ME^2 project under contract no. 11227902 from the National Natural Science Foundation of China.

Author affiliations: [a]Key Laboratory of Quantum Materials and Devices of Ministry of Education, School of Physics, Southeast University, Nanjing 211189, China; [b]School of Physics and Astronomy, Shanghai Jiao Tong University, Shanghai 200240, China; [c]National Synchrotron Radiation Laboratory, University of Science and Technology of China, Hefei 230029, China; [d]Advanced Light Source, Lawrence Berkeley National Laboratory, Berkeley, CA 94720; [e]Wuhan National High Magnetic Field Center & School of Physics, Huazhong University of Science and Technology, Wuhan 430074, China; [f]Department of Physics, New York University, New York, NY 10003; [g]Collaborative Innovation Center of Advanced Microstructures, Nanjing University, Nanjing 210093, China; and [h]Tsung-Dao Lee Institute, Shanghai Jiao Tong University, Shanghai 200240, China

1. M. Imada, A. Fujimori, Y. Tokura, Metal–insulator transitions. *Rev. Mod. Phys.* **70**, 1039 (1998).
2. V. Dobrosavljevic, N. Trivedi, J. M. Valles Jr., *Conductor-Insulator Quantum Phase Transitions* (Oxford University Press, 2012).
3. P. Sun, M. Søndergaard, B. Iversen, F. Steglich, Strong electron correlations in $FeSb_2$. *Annalen der Physik* **523**, 612 (2011).
4. C. Petrovic *et al.*, Anisotropy and large magnetoresistance in the narrow-gap semiconductor $FeSb_2$. *Phys. Rev. B* **67**, 155205 (2003).
5. A. Bentien, S. Johnsen, G. K. H. Madsen, B. B. Iversen, F. Steglich, Colossal Seebeck coefficient in strongly correlated semiconductor $FeSb_2$. *EPL* **80**, 17008 (2007).
6. P. Sun, N. Oeschler, S. Johnsen, B. B. Iversen, F. Steglich, Huge thermoelectric power factor: $FeSb_2$ versus $FeAs_2$ and $RuSb_2$. *Appl. Phys. Express* **2**, 091102 (2009).
7. C. Petrovic *et al.*, Kondo insulator description of spin state transition in $FeSb_2$. *Phys. Rev. B* **72**, 045103 (2005).
8. M. K. Fuccillo, Q. D. Gibson, M. N. Ali, L. M. Schoop, R. J. Cava, Correlated evolution of colossal thermoelectric effect and Kondo insulating behavior. *APL Mater.* **1**, 062102 (2013).
9. M. S. Figueira, J. Silva-Valencia, R. Franco, Thermoelectric properties of the Kondo insulator $FeSb_2$. *Eur. Phys. J. B* **85**, 203 (2012).
10. Z. Schlesinger, Z. Fisk, H.-T. Zhang, M. Maple, Is FeSi a Kondo insulator? *Phys. B: Condens. Matter* **237–238**, 460 (1997).
11. C. M. Varma, Aspects of strongly correlated insulators. *Phys. Rev. B* **50**, 9952 (1994).
12. J. M. Tomczak, K. Haule, G. Kotliar, Signatures of electronic correlations in iron silicide. *Proc. Natl. Acad. Sci. U.S.A.* **109**, 3243 (2012).
13. K.-J. Xu *et al.*, Metallic surface states in a correlated *d*-electron topological Kondo insulator candidate $FeSb_2$. *Proc. Natl. Acad. Sci. U.S.A.* **117**, 15409 (2020).
14. A. J. Breindel *et al.*, Probing FeSi, a *d*-electron topological Kondo insulator candidate, with magnetic field, pressure, and microwaves. *Proc. Natl. Acad. Sci. U.S.A.* **120**, e2216367120 (2023).
15. M. A. Korotin *et al.*, Intermediate-spin state and properties of $LaCoO_3$. *Phys. Rev. B* **54**, 5309 (1996).
16. K. Asai *et al.*, Two spin-state transitions in $LaCoO_3$. *J. Phys. Soc. Jpn.* **67**, 290 (1998).
17. M. W. Haverkort *et al.*, Spin state transition in $LaCoO_3$ studied using soft X-ray absorption spectroscopy and magnetic circular dichroism. *Phys. Rev. Lett.* **97**, 176405 (2006).
18. D. Takegami *et al.*, Paramagnetic $LaCoO_3$: A highly inhomogeneous mixed spin-state system. *Phys. Rev. X* **13**, 011037 (2023).
19. A. Farhan, M. Reissner, A. Leithe-Jasper, W. Steiner, A high-field Mössbauer investigation on $FeSb_2$. *J. Phys. Conf. Ser.* **217**, 012142 (2010).
20. F. Hulliger, E. Mooser, Semiconductivity in pyrite, marcasite and arsenopyrite phases. *J. Phys. Chem. Solids* **26**, 429 (1965).
21. J. B. Goodenough, Energy bands in TX_2 compounds with pyrite, marcasite, and arsenopyrite structures. *J. Solid State Chem.* **5**, 144 (1972).
22. T. B. E. Grønbech *et al.*, Chemical bonding in colossal thermopower $FeSb_2$. *Chem. Eur. J.* **26**, 8651 (2020).
23. A. Bentien, G. K. H. Madsen, S. Johnsen, B. B. Iversen, Experimental and theoretical investigations of strongly correlated $FeSb_{2-x}Sn_x$. *Phys. Rev. B* **74**, 205105 (2006).
24. A. Chikina *et al.*, Correlated electronic structure of colossal thermopower $FeSb_2$: An ARPES and ab initio study. *Phys. Rev. Res.* **2**, 023190 (2020).
25. J. Shen *et al.*, Robust Fe divalent state in one-unit-cell FeSe/SrTiO3 thin films. *Phys. Rev. B* **106**, 245112 (2022).
26. W. L. Yang *et al.*, Evidence for weak electronic correlations in iron pnictides. *Phys. Rev. B* **80**, 014508 (2009).
27. P. Sun *et al.*, Magnetism and Spin States of $FeSb_2$. *Sci. Rep.* **55** (2011).
28. P. S. Miedema, F. M. de Groot, The iron L edges: Fe 2p X-ray absorption and electron energy loss spectroscopy. *J. Electron Spectrosc. Relat. Phenom.* **187**, 32 (2013).
29. L. Kipgen *et al.*, Evolution of cooperativity in the spin transition of an iron (II) complex on a graphite surface. *Nat. Commun.* **9**, 2984 (2018).
30. M. L. Baker *et al.*, K- and L-edge X-ray absorption spectroscopy (XAS) and resonant inelastic X-ray scattering (RIXS) determination of differential orbital covalency (DOC) of transition metal sites. *Coord. Chem. Rev.* **345**, 182 (2017).
31. A. G. Eaton *et al.*, Electrical transport signatures of metallic surface state formation in the strongly-correlated insulator $FeSb_2$. arXiv [Preprint] (2024). https://doi.org/10.48550/arXiv.2403.04550
32. Y. S. Eo *et al.*, Extraordinary bulk-insulating behavior in the strongly correlated materials FeSi and $FeSb_2$. *Appl. Phys. Lett.* **122**, 233102 (2023).
33. B. Gorshunov *et al.*, Low-energy electrodynamics of SmB_6. *Phys. Rev. B* **59**, 1808 (1999).
34. H. Takahashi, R. Okazaki, I. Terasaki, Y. Yasui, Origin of the energy gap in the narrow-gap semiconductor $FeSb_2$ revealed by high-pressure magnetotransport measurements. *Phys. Rev. B* **88**, 165205 (2013).
35. Q. Du, X. Tong, Y. Liu, C. Petrovic, Suppression of thermal conductivity and electronic correlations in $Fe_{1-x}Ru_xSb_2$ ($0 \leq x \leq 0.6$). *Appl. Phys. Lett.* **118**, 171904 (2021).
36. A. Herzog *et al.*, Strong electron correlations in $FeSb_2$: An optical investigation and comparison with $RuSb_2$. *Phys. Rev. B* **82**, 245205 (2010).
37. Z. P. Yin, K. Haule, G. Kotliar, Kinetic frustration and the nature of the magnetic and paramagnetic states in iron pnictides and iron chalcogenides. *Nat. Mater.* **10**, 932 (2011).
38. K. Haule, T. Birol, Free energy from stationary implementation of the DFT+DMFT functional *Phys. Rev. Lett.* **115**, 256402 (2015).
39. P. G. Radaelli, S. W. Cheong, Structural phenomena associated with the spin-state transition in $LaCoO_3$. *Phys. Rev. B* **66**, 094408 (2002).
40. C. C. Homes *et al.*, Unusual electronic and vibrational properties in the colossal thermopower material $FeSb_2$. *Sci. Rep.* **8**, 11692 (2018).
41. S. Noguchi, S. Kawamata, K. Okuda, H. Nojiri, M. Motokawa, Evidence for the excited triplet of Co^{3+} in $LaCoO_3$. *Phys. Rev. B* **66**, 094404 (2002).
42. H. Takahashi *et al.*, Colossal Seebeck effect enhanced by quasi-ballistic phonons dragging massive electrons in $FeSb_2$. *Nat. Commun.* **7**, 12732 (2016).
43. I. I. Mazin, K. Koepernik, M. D. Johannes, R. González-Hernández, L. Šmejkal, Prediction of unconventional magnetism in doped $FeSb_2$. *Proc. Natl. Acad. Sci. U.S.A.* **118**, e2108924118 (2021).
44. Z. Schlesinger *et al.*, Unconventional charge gap formation in FeSi. *Phys. Rev. Lett.* **71**, 1748 (1993).
45. L. A. Wray *et al.*, Measurement of the spectral line shapes for orbital excitations in the Mott insulator CoO using high-resolution resonant inelastic x-ray scattering. *Phys. Rev. B* **88**, 035105 (2013).
46. L. Miao *et al.*, High temperature singlet-based magnetism from Hund's rule correlations. *Nat. Commun.* **10**, 644 (2019).
47. R. D. Cowan, "Robert d. cowan's atomic structure code" (2009) https://www.tcd.ie/Physics/people/Cormac.McGuinness/Cowan/.
48. E. Anderson *et al.*, *LAPACK's User's Guide* (Society for Industrial and Applied Mathematics, 1992).
49. G. Kresse, J. Furthmüller, Efficient iterative schemes for *ab initio* total-energy calculations using a plane-wave basis set. *Phys. Rev. B* **54**, 11169 (1996).
50. G. Kresse, J. Furthmüller, Efficiency of *ab-initio* total energy calculations for metals and semiconductors using a plane-wave basis set. *Comput. Mater. Sci.* **6**, 15 (1996).
51. J. P. Perdew, K. Burke, M. Ernzerhof, Generalized gradient approximation made simple. *Phys. Rev. Lett.* **77**, 3865 (1996).
52. A. I. Liechtenstein, V. I. Anisimov, J. Zaanen, Density-functional theory and strong interactions: Orbital ordering in Mott–Hubbard insulators. *Phys. Rev. B* **52**, R5467–R5470 (1995).